Analyst

RSC Publishing

PAPER

View Article Online
View Journal | View Issue

Cite this: *Analyst*, 2013, **138**, 7206

High-performance H_2S detection by redox reactions in semiconducting carbon nanotube-based devices†

Hyun Young Jung,*[a] Young Lae Kim,[a] Sora Park,[b] Aniket Datar,[ac] Hyung–June Lee,[b] Jun Huang,[ac] Sivasubramanian Somu,[ac] Ahmed Busnaina,[ac] Yung Joon Jung[ab] and Young–Kyun Kwon*[b]

Received 14th September 2013
Accepted 26th September 2013

DOI: 10.1039/c3an01762a

www.rsc.org/analyst

Here we report the highly effective detection of hydrogen sulfide (H_2S) gas by redox reactions based on single-walled carbon nanotubes (SWCNTs) functionalized with 2,2,6,6-tetramethylpiperidine-1-oxyl (TEMPO) as a catalyst and we also discuss the important role of water vapor in the electrical conductivity of SWCNTs during the sensing of H_2S molecules. To explore the H_2S sensing mechanism, we investigate the adsorption properties of H_2S on carbon nanotubes (CNTs) and the effects of the TEMPO functionalization using first-principles density functional theory (DFT) and we summarize current changes of devices resulting from the redox reactions in the presence of H_2S. The semiconducting-SWCNT (s-SWCNT) device functionalized with TEMPO shows a very high sensitivity of 420% at 60% humidity, which is 17 times higher than a bare s-SWCNT device under dry conditions. Our results offer promising prospects for personal safety and real-time monitoring of H_2S gases with the highest sensitivity and low power consumption and potentially at a low cost.

Introduction

Hydrogen sulfide (H_2S) is a deadly gas which causes asphyxiation, lung damage, and teratogenic effects when exposed to it.[1,2] Thus the monitoring and elimination of H_2S is very important for safety because this gas is found widely in industry such as in natural gas, petroleum and mines, and is given off as a by-product in the manufacture of rayon, synthetic rubber, dyes and the tanning of leather.[3,4] So far wide varieties of inorganic and organic materials such as tungsten oxide, tin oxide and carbon have been proposed as electrical sensors that can detect the H_2S gas.[5–8] Although there are several successful devices available commercially, drawbacks of existing H_2S monitors include high power consumption, high operating temperatures, short lifetime, interference from other gases and high cost.[9]

Recently there has been significant interest in using carbon based nanomaterials as chemical sensors due to several advantages of nanostructured carbon such as light weight, high electrical conductivity, electrochemical surface area and superior sensing performance. Particularly, carbon nanotubes (CNTs) are in growing demand due to their high electron mobility and large current capability,[10,11] which, on one hand, can potentially help in reducing the power consumption of the sensor whereas, on the other hand, high temperature stability and chemical inertness of CNTs may provide a stable and robust platform to detect specific gas.[12–24] Since pristine CNT based chemical sensors utilize their intrinsic electrochemical properties to overcome their limitations in selectivity and sensitivity, the most promising approach is to functionalize CNTs with covalent or non-covalent materials.[24–33] However owing to their one-dimensional nanostructure, CNTs are highly sensitive to environments such as humidity and temperature,[34,35] in practice the effect of the relative humidity (RH) on CNT based chemical sensors must be investigated further because the humidity varies greatly depending on the season, region and weather.

Here, we report molecular doping of 2,2,6,6-tetramethylpiperidine-1-oxyl (TEMPO) as a catalyst on the surface of single-walled carbon nanotubes (SWCNTs) and the effective detection of H_2S gas by a redox reaction at room temperature. We also discuss the important role of water vapor in the electrical conductivity of SWCNTs during the sensing of H_2S molecules.

Experimental

Fabrication of SWCNT arrays on a substrate

First, a plasma treatment is used to enhance the hydrophilic nature of the SiO_2 surface. To improve the contact between the SWCNT-deionized water solution and substrate, the substrate was pretreated using an Inductively-Coupled Plasma (ICP) with

[a]*Department of Mechanical and Industrial Engineering, Northeastern University, Boston, MA 02115, USA. E-mail: hjung@coe.neu.edu*

[b]*Department of Physics, Research Institute for Basic Sciences, Kyung Hee University, Seoul 130–701, Korea. E-mail: ykkwon@khu.ac.kr*

[c]*NSF Nanoscale Science and Engineering Center for High–Rate Nanomanufacturing, Northeastern University, Boston, MA 02115, USA*

† Electronic supplementary information (ESI) available: Additional experimental data (Fig. S1–S9), and a table displaying reduction and oxidation potential values. See DOI: 10.1039/c3an01762a

mixed gas flow of O_2 (20 sccm), SF_6 (20 sccm), and Ar (5 sccm). Second, 600 nm thick PMMA photoresist patterns are constructed using electron-beam lithography (EBL) to build nanoscale channels which form templates for building the interconnect architectures. Next, these templated substrates are dip-coated in a SWCNT-DI water solution (purchased from Brewer Sci. Inc. and used as is) at a constant pulling rate of 0.1 mm min^{-1}, which resulted in organized and aligned SWCNT networks having well-defined shapes at micro- and nano-scale and were defined by the geometry of PMMA patterns on the substrate.[36,37] After the SWCNT assembly, contact pads or electrodes were deposited. Initially a 5 nm Ti layer was deposited followed by a 150 nm Au layer. Au contacts were then wire bonded. Here, SWCNTs serve as an active channel layer because of their ultra-high surface area to volume ratio and no chemical interaction with H_2S or other gases that may interfere.

Standard lab preparation of H_2S gas molecules

For generation of H_2S gas, ferrous sulfide (FeS, purchased from Sigma-Aldrich) was reacted with sulfuric acid. $FeS(s) + H_2SO_4(aq) \rightarrow FeSO_4(s) + H_2S(g)$. Because H_2S gas is denser than air, it is more convenient to collect it in a glass vial by downward delivery. The gas produced in a chemical reaction is passed through a delivery tube into the glass vial, where it sinks and pushes the air out of the top. Calculated volumes of the H_2S were then introduced into 1 L of a gas sensing chamber using a microliter syringe.

Gas detection using SWCNT (w/wo TEMPO) devices on finger electrodes

In order to investigate the sensing mechanism and improve sensitivity, we compared sensor performances between semiconducting SWCNT (s-SWCNT) and metallic SWCNT (m-SWCNT) devices with and without TEMPO functionalization and studied the behavior of H_2S and H_2O molecules. Here, s-SWCNTs play a major role in gas detection due to their different redox properties.[38,39] For this, we performed a controlled experiment where 99% purity 10 mL m-SWCNT and s-SWCNT nanotube solutions (purchased from NanoIntegris Inc.) were drop-cast on each inter-digitated finger electrodes (ESI Fig. S1†). The solution was allowed to dry and was rinsed with water to remove surfactants until maximum current was recorded. After this step, the devices were exposed to TEMPO vapors for 15 min. The devices were then cooled down at room temperature and allowed to equilibrate for an additional 30 min. For gas sensing, each device was carefully outgassed by joule heating under 10^{-3} torr for 1 h in a sensing chamber followed by a flow of dry N_2 gas. The gas chamber was then closed and a pre-calculated amount of H_2S gas was introduced in it. The applied bias voltage was kept constant for every measurement and changes in current were monitored as a function of time for different gas concentrations. To understand the effects of concentration of H_2S gas, the sensor devices were exposed to H_2S gas of 5, 10, 50, 100, and 200 ppm, respectively, in the chamber with dry N_2. To investigate the effect of H_2O on sensing of H_2S molecules, 100 ppm H_2S gas was introduced in the presence of 20, 40 and 60% RH. Changes in current were observed until it reached saturation. Once the current saturated, the chamber was exposed to dry N_2 for the sensor recovery. In graphs of the real-time current changes, a sharp decrease in current indicates the sensor response to H_2S gas when a certain amount of H_2S gas is injected into the closed chamber. The current increases when the sensor is allowed to recover in N_2 gas.

Computational methods

To explore the chemical reaction of H_2S, O_2, and TEMPO molecules, we performed the first-principles calculations based on density functional theory (DFT) implemented in the DMol^3 package.[40] We used the generalized gradient approximation (GGA) with the Perdew–Burke–Ernzerhof (PBE) functional[41] to describe the exchange-correlation (XC) functional. A double numerical polarized basis set was chosen with a real-space cutoff of 4.0 Å to expand the electronic wave functions. The octupole scheme for the multipolar fitting procedure and a fine grid scheme for the numerical integration were employed for an accurate evaluation of the charge density. To search for a three-dimensional trajectory for the reaction path between reactants and products during the chemical reaction, the linear synchronous transit and quadratic synchronous transit (LST/QST) calculations[42,43] were carried out with conjugate gradient minimization.[44]

Results and discussion

Experimental setup and H_2S gas detection

Fig. 1a–d show the scanning electron microscope (SEM) images of the experimental setup for H_2S gas detection. We assembled SWCNT microarrays by a template guided fluidic assembly process in order to obtain uniform networks[36,37] and then

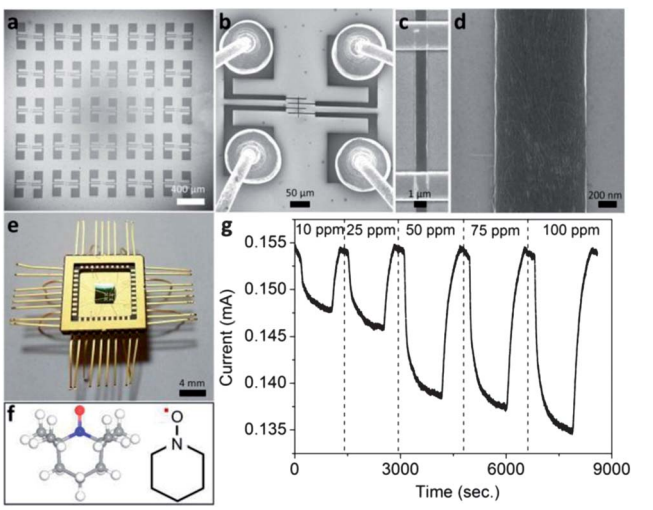

Fig. 1 (a–d) The scanning electron microscope (SEM) images of the experimental setup for assembled SWCNT array devices. (e) An optical image of wafer scale sensor devices. (f) Chemical structure of TEMPO molecules. (g) Real-time current changes as a function of concentration of H_2S gas at 10, 25, 50, 75 and 100 ppm for the functionalized SWCNT sensor.

electrodes were formed on top of them (see Experimental section for more details). Such a process allowed us to assemble SWCNT network arrays with very precise control over placement and density of SWCNTs over wafer scale (Fig. 1e). Fig. 1f shows the chemical structure of TEMPO molecules. SWCNTs serve as an active channel layer because of their ultra-high surface area to volume ratio and no chemical interaction with H_2S or other gases that may interfere. Since TEMPO possesses a stable nitroxyl group provided by the adjacent four methyl groups, it has widely been used as a radical trap, as a structural probe for biological systems, as a reagent in organic synthesis, and as a mediator in controlled free radical polymerization.[45–48] Thus it is also capable of oxidizing the gaseous H_2S and can be utilized as a sensory molecule for making a chemical sensor to detect H_2S.

We exposed the non-covalently functionalized SWCNT devices to different concentrations of H_2S gas ranging from 10–100 ppm. The applied bias voltage was kept constant for every measurement and changes in current were monitored as a function of time for different gas concentrations. Fig. 1g shows the current *vs.* time plot for the functionalized SWCNT sensor when exposed to different concentrations of H_2S gases. The sharp decrease in current indicates the sensor response to H_2S gas when a certain amount of H_2S gas is injected into the closed chamber. When the chamber is opened and the sensor is allowed to recover in open air, the current increases to approximately its previous level before exposure to H_2S gas. For each concentration of H_2S, we evaluated sensitivity S defined by $S = \{(R_{gas} - R_i)/R_i\} \times 100 = \{(I_i - I_{gas})/I_{gas}\} \times 100$, where I_i is the initial current and I_{gas} is the changed current after injection of H_2S gas. The sensitivity of the functionalized SWCNT arrays shows a 4.7% change at 10 ppm and 13.7% at 100 ppm.

Sensing of H_2S molecules by redox reactions

In order to investigate the sensing mechanism and improve sensitivity, we compared sensor performances between semiconducting SWCNT (s-SWCNT) and metallic SWCNT (m-SWCNT) devices with and without TEMPO functionalization and studied the behavior of H_2S and H_2O molecules. Here, s-SWCNTs play a major role in gas detection due to their different redox properties.[49,50] For this, we performed a controlled experiment where 99% purity m-SWCNT and s-SWCNT nanotube solutions (purchased from NanoIntegris Inc.) were drop-cast on each inter-digitated finger electrode (ESI Fig. S1†). Then we functionalized the SWCNT based devices with TEMPO using a vaporization method to achieve uniform and thin coating for the functionalization of SWCNTs, which was then carefully outgassed by joule heating under 10^{-3} torr for 1 h followed by injection of dry N_2 gas in a sensing chamber. Non-covalently functionalized SWCNT devices were exposed to H_2S gas under dry N_2 or controlled water vapor. Clearly, in all the above-mentioned detections, the sensing materials come in contact with either H_2O or H_2S or a mixture of these two.

Fig. 2 shows sensing of H_2S molecules with SWCNT devices and the effect of relative humidity. In order to investigate the exact sensing mechanism and interactions between SWCNT–TEMPO–H_2S–H_2O, we compared sensor performances in the

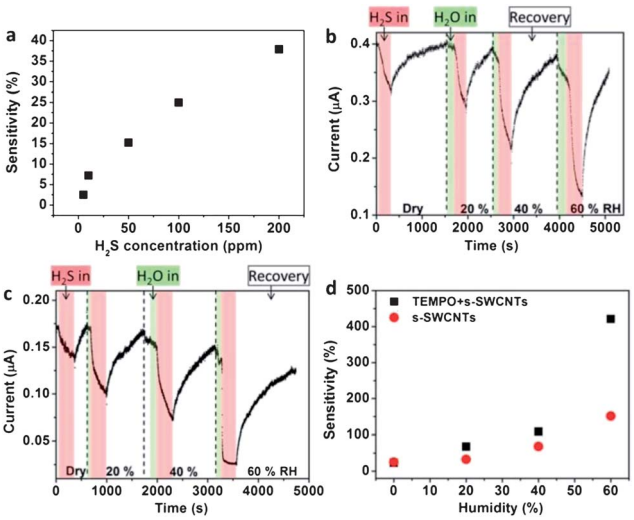

Fig. 2 Sensitivity and real-time current measurements for detection of H_2S gas. (a) Sensitivity of a bare s-SWCNT device as a function of H_2S concentration. Real-time current measurement of (b) a bare s-SWCNT device and (c) a device functionalized with TEMPO as a function of RH. (d) Sensitivity of B and C. In the range of current reduction of B and C, red and green areas mean injection of H_2S and H_2O molecules respectively, and the increase of current indicates recovery into the initial current value of each RH.

absence or presence of water between s-SWCNT and m-SWCNT devices which are either functionalized by TEMPO or not. First, to understand the effects of H_2S gas on a bare SWCNT, SWCNT-based sensor devices without TEMPO functionalization were exposed to H_2S gas of 5, 10, 50, 100, and 200 ppm, respectively in the chamber with dry N_2. Fig. 2a shows the sensitivity of the bare s-SWCNT device with H_2S concentration in dry N_2 (ESI Fig. S2† for real time current change). The sensitivity at 200 ppm of H_2S shows 38% change. However, the bare m-SWCNT device shows less than 5% sensitivity (ESI Fig. S2†) on detecting H_2S gases. This result is consistent with previous reports,[6] indicating more redox properties of the s-SWCNTs.

To investigate the effect of H_2O on sensing of H_2S molecules, we used only 100 ppm concentration of H_2S since it is known that, above this concentration, the human olfactory nerve can be paralyzed in a few inhalations. Then sensing of H_2S gas was performed at different RH. Fig. 2b shows the real-time current changes in a bare s-SWCNT device when 100 ppm H_2S gases were exposed at an RH of 0, 20, 40 and 60% (ESI Fig. S4† for more details and ESI Fig. S5† for the bare m-SWCNT device). First, we observed that the current in the s-SWCNT device decreased when exposed to water vapor. Then a further substantial reduction in conductance was observed when H_2S gas was introduced in the presence of predetermined RH. After each sensing test at a given RH, the chamber was exposed to dry N_2 for the sensor recovery for sensing of H_2S in increased RH. The real-time current measurements clearly demonstrate that redox properties do change in the presence of H_2S and water vapor. The sensitivity of bare s-SWCNT devices was increased significantly to 150% at 60% RH (Fig. 2d).

H_2O molecules can be adsorbed on the surface of SWCNTs and act as electron donors in a p-type semiconductor reducing

the hole density in s-SWCNTs resulting in the current decreases.[34] To explain the increased H_2S sensitivity of s-SWCNTs, the interaction of H_2S and H_2O molecules is a possible subset. Because the moisture concentration of 60% RH at 20 °C is about 0.01 g in 1 L of the chamber, the amount of water molecules will decide the sensing reaction. Therefore, the conductance after injection of H_2S gas can be changed significantly by more water molecules at higher RH. Moreover, the redox reactions with TEMPO can additionally generate more water molecules as shown in Fig. 3a. This indicates that moisture is one of the important factors in practical applications and sensitivity of the chemical sensors.

To maximize sensitivity based on the above facts, TEMPO was used as a homogeneous catalyst for redox reaction of H_2S and H_2O. As shown in Fig. 2c and d (ESI Fig. S7† for more details), s-SWCNT devices functionalized with TEMPO showed 420% sensitivity at 60% RH, which is about 3 times higher than that of the bare s-SWCNT sensor at the same RH, and 17 times higher than that of the bare s-SWCNT device under dry N_2 conditions.

Redox reactions and sensing mechanism

To understand the underlying sensing mechanism, we paid close attention to the redox reactions of various molecules existing near active CNT channels (see ESI Table S1†), which exhibit p-type characteristics under ambient conditions. This is attributed to the fact that the CNT is p-doped due to the oxygen adsorption,[51,52] where each O_2 molecule takes an electron away from or donates a hole to the CNT. These adsorbed O_2 molecules exist in the form of O_2^- and will participate in our proposed redox reaction by donating electrons back to the CNTs resulting in less p-doped CNT channels.

Fig. 3a shows a schematic of a full cycle of the redox reactions that we propose to occur for H_2S detection near the CNT channel functionalized by TEMPO under humid conditions. In the first stage of the redox reactions, TEMPO is oxidized to be $TEMPO^+$ with positive charge, which is an important product for H_2S dissociation, while H_2O molecules with O_2 molecules from O_2^- reduce. At the second stage of the redox reactions, the reduction reaction of $TEMPO^+$ to TEMPO–H is coupled to the dissociation process of H_2S to $S + 2H^+ + 2e^-$. In the final stage of the redox reaction cycle, the sulfur atoms produced by the latter reaction in the second stage react with oxygen ions (O_2^-) responsible for the p-type characteristics of CNT devices and thus form various sulfuric oxides such as SO, SO_2 as the oxidation reaction during which the remaining electrons are back-donated to the CNT channels is less p-type. In the counter reduction reaction, TEMPO–H becomes back to TEMPO in the presence of other TEMPO molecules, and the detached H atoms may be involved in the formation of H_2SO_4 from the sulfuric oxides. Through such a complete reactions cycle, the TEMPO molecules together with water play a significant catalytic role in H_2S detection.

For further analysis, we investigated the chemical reaction barriers of H_2S, O_2 and TEMPO molecules functionalized on the CNT surface using first-principles density functional theory (DFT) (see Experimental section for computational methods). Fig. 3b shows a schematic diagram of the energy profile along the reaction coordinates exhibiting an activation barrier (E_a) in the chemical reactions between H_2S and O_2 molecules without/with TEMPO molecules. The reaction energies (E_r) are defined by the energy difference between the reactant and the product. We considered the initial geometries of H_2S and O_2 molecules without/with TEMPO molecules functionalizing the CNT surface and the optimized final structures of H_2SO_4 molecules. We obtained the interpolated pathway determined geometrically using linear synchronous transit (LST),[53] and calculated E_a and E_r of the reaction. O_2 molecules on the CNT surface could interact with H_2S as well as H_2O molecules. The chemical reaction between H_2S and O_2 would eventually produce H_2SO_4. As a result, p-doped CNT surfaces by oxygen were deoxidized with reduction of the hole carrier density and thus the current in CNT devices. Although the schematic reaction diagram shown in Fig. 3b represents an oversimplified reaction path to produce H_2SO_4 from H_2S and thus cannot be matched with any reaction in the redox cycle, our calculations used for this diagram verifies an important catalytic behavior of TEMPO molecules. The activation barrier of 5.40 eV without TEMPO decreases by about 34% to be 3.56 eV with TEMPO implying that the presence of TEMPO may expedite the chemical reactions involving H_2S, O_2, H_2O, *etc.*, leading to the improvement of sensitivity.

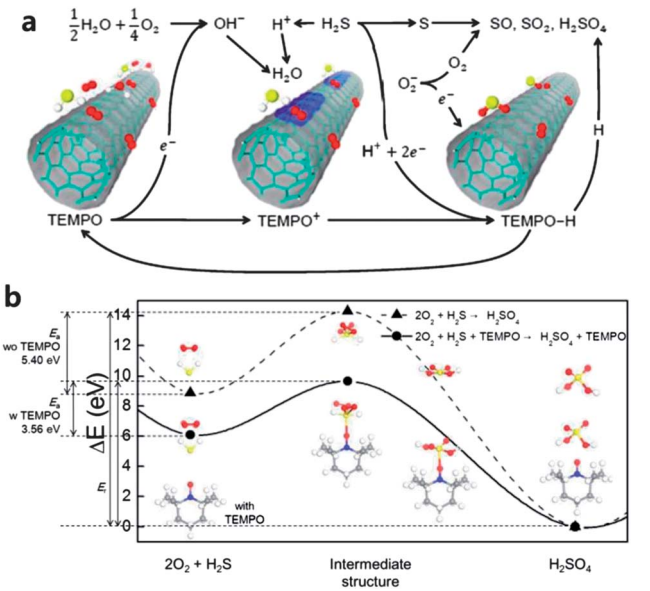

Fig. 3 (a) Schematic of redox reactions of H_2S on p-doped CNT (due to, for example, O_2 adsorption) with TEMPO functionalization in the presence of H_2O. See the text for detailed description of the reactions. (b) A schematic diagram of the energy profiles along the reaction coordinates exhibiting an activation barrier (E_a) in the chemical reactions. The dashed line with triangles represents the energy profile of the chemical reactions between H_2S and O_2 molecules without TEMPO, while the solid line with circles does the same with TEMPO. The energies of initial structures and final structures are the sum of the energies of isolated component molecules. TEMPO takes a part in the reaction as a catalyst resulting in the diminution of the activation barrier by about 34%. Molecular structures in the chemical reactions are shown as the inset, where the red dots represent oxygen atoms, the yellow ones sulfur, and the white one hydrogen.

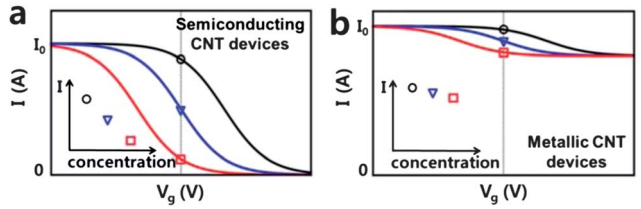

Fig. 4 Change in the I–V_g characteristic curves of (a) s-CNT and (b) m-CNT devices resulting from the redox reactions in the presence of H_2S. The inset in each graph schematically represents the current as a function of H_2S concentration.

Based on our proposed sensing mechanism, we present the presumed changes of I–V_g characteristics due to H_2S in Fig. 4. The black curves in Fig. 4a and b represent I–V_g characteristics of typical semiconducting and metallic devices, respectively, in the absence of H_2S. Note that the s-SWCNT device (Fig. 4a) exhibits a very high on–off ratio, while the on–off ratio of the m-SWCNT device (Fig. 4b) is close to one. In the presence of H_2S, the redox reactions cause the electron back donation to CNT devices making them less p-doped as discussed above, resulting in I–V_g curves to be shifted to the left. Since the amount of the electron back-donation is proportional to the concentration of H_2S, the higher the H_2S concentration, the more to the left the I–V_g curve is shifted. For a given gate bias (usually zero bias), the measured current decreases with the H_2S concentration from the black circle to the blue triangle to the red square in Fig. 4a and b. As clearly seen in the figure, we attribute much higher sensitivity in semiconducting CNT devices than in metallic devices to the significant difference in their on–off ratios. Our proposed sensing mechanism also explains the humidity effects. The initial conductance drop by H_2O seen in our measurements is caused by the first stage of the redox reactions as described in Fig. 3a. The H_2S sensitivity enhancement in the humid conditions with high RH can be elucidated by the fact that the reaction of TEMPO to $TEMPO^+$ may increase with humidity.

Conclusions

In summary, to date, there has been a dearth of studies on the role of relative humidity in H_2S gas detection. The SWCNT device functionalized with TEMPO highly responded to H_2S gas in water vapor. Its reactivity depends on the electronic properties of the active channel, especially s-SWCNTs showed a very high sensitivity of 420% at 60% humidity. Our sensors offer promising prospects for real-time monitoring of H_2S gas not only with very high sensitivity and low power consumption, but potentially also at a low cost. The small size of the system will also allow future integration with low power microelectronics.

Acknowledgements

The Northeastern University authors acknowledge support from Advanced Energy Consortium, and the National Science Foundation Nanoscale Science and Engineering Center (NSEC) for High-rate Nanomanufacturing (NSF grant-EEC-0832785). The experiments were conducted at the George J Kostas Nanoscale Technology and Manufacturing Research Center. The Kyung Hee University authors gratefully acknowledge the financial support from the National Research Foundation of Korea (Grant no. 2011-0002456 and 2012-0005146). Some portion of our computational work was done using the resources of the KISTI Supercomputing Center (KSC-2012-C2-72 and KSC-2013-C2-024).

Notes and references

1 H. Peng, Y. Cheng, C. Dai, A. L. King, B. L. Predmore, D. Lefer and B. Wang, *Angew. Chem., Int. Ed.*, 2011, **50**, 9672–1975.
2 K. Abe and H. Kimura, *J. Neurosci.*, 1996, **16**, 1066–1071.
3 G. Wesenberg and N. H. Proctor, *Chemical Hazards of the workplace*, Wiley, 4th edn, New York, 1996.
4 B. Yang, S. Wang, S. Tian and L. Liu, *Electrochem. Commun.*, 2009, **11**, 1230–1233.
5 S. Chen, Z. Chen, W. Ren and H. Ai, *J. Am. Chem. Soc.*, 2012, **134**, 9589–9592.
6 D. R. Kauffman and A. Star, *Angew. Chem., Int. Ed.*, 2008, **47**, 6550–6570.
7 S. Mubeen, T. Zhang, N. Chartuprayoon, Y. Rheem, A. Mulchandani, N. V. Myung and M. A. Deshusses, *Anal. Chem.*, 2010, **82**, 250–257.
8 Z. Sun, H. Yuan, Z. Liu, B. Han and X. Zhang, *Adv. Mater.*, 2005, **17**, 2993–2997.
9 A. Chowdhuri, V. Gupta, K. Sreenivas, R. Kumar, S. Mozumdar and P. K. Patanjali, *Appl. Phys. Lett.*, 2004, **84**, 1180.
10 M. Lee, M. Noah, J. Park, M.-J. Seong, Y.-K. Kwon and S. Hong, *Small*, 2009, **5**, 1642–1648.
11 M. Lee, K. Y. Baik, M. Noah, Y.-K. Kwon, J.-O. Lee and S. Hong, *Lab Chip*, 2009, **9**, 2267–2280.
12 M. S. Strano, C. A. Dyke, M. L. Usrey, P. W. Barone, M. J. Allen, H. Shan, C. Kittrell, R. H. Hauge, J. M. Tour and R. E. Smalley, *Science*, 2003, **301**, 1519–1522.
13 E. S. Snow, F. K. Perkins, E. J. Houser, S. C. Badescu and T. L. Reinecke, *Science*, 2005, **307**, 1942–1945.
14 J. Kong, N. R. Franklin, C. W. Zhou, M. G. Chapline, S. Peng, K. J. Cho and H. Dai, *Science*, 2000, **287**, 622–625.
15 G. Jimenez-Cadena, J. Riu and F. X. Rius, *Analyst*, 2007, **132**, 1083–1099.
16 P. Vichchulada, Q. Zhang and M. D. Lay, *Analyst*, 2007, **132**, 719–723.
17 I. Sasaki, N. Minami, A. Karthigeyan and K. Iakoubovskii, *Analyst*, 2009, **134**, 325–330.
18 X. Tang, S. Bansaruntip, N. Nakayama, E. Yenilmez, Y. Chang and Q. Wang, *Nano Lett.*, 2006, **6**, 1632–1636.
19 T. Kawano, H. C. Chiamori, M. Suter, Q. Zhou, B. D. Sosnowchik and L. Lin, *Nano Lett.*, 2007, **7**, 3686–3690.
20 E. J. Parra, F. X. Rius and P. Blondeau, *Analyst*, 2013, **138**, 2698–2703.
21 M. C. McAlpine, H. Ahmad, D. Wang and J. R. Heath, *Nat. Mater.*, 2007, **6**, 379–384.
22 H.-J. Lee, G. Kim and Y.-K. Kwon, *Chem. Phys. Lett.*, 2013, **580**, 57–61.

23 B. Y. Lee, M. G. Sung, J. Lee, K. Y. Baik, Y.-K. Kwon, M.-S. Lee and S. Hong, *ACS Nano*, 2011, **5**, 4373–4379.
24 H. J. Song, Y. Lee, T. Jiang, A.-G. Kussow, M. Lee, S. Hong, Y.-K. Kwon and H. C. Choi, *J. Phys. Chem. C*, 2008, **112**, 629–634.
25 C. M. Hussain, C. Saridara and S. Mitra, *Analyst*, 2009, **134**, 1928–1933.
26 P. W. Barone and M. S. Strano, *Angew. Chem., Int. Ed.*, 2006, **45**, 8138–8141.
27 R. Haddad, S. Cosnier, A. Maaref and M. Holzinger, *Analyst*, 2009, **134**, 2412–2418.
28 M. K. Kumar and S. Ramaprabhu, *J. Phys. Chem. B*, 2006, **110**, 11291–11298.
29 Z. Zanoll, R. Leghrib, A. Felten, J. Pireaux, E. Llobet and J. Charlier, *ACS Nano*, 2011, **5**, 4592–4599.
30 A. Star, V. Joshi, S. Skarupo, D. Thomas and J. P. Gabriel, *J. Phys. Chem. B*, 2006, **110**, 21014–21020.
31 C.-W. Liang, S. Sahakalkan and S. Roth, *Small*, 2008, **4**, 432–436.
32 Y. Sun and H. H. Wang, *Adv. Mater.*, 2007, **19**, 2818–2823.
33 Y. Lu, M. Meyyappan and J. Li, *Small*, 2011, **7**, 1714–1718.
34 A. Zahab, N. Spina and P. Poncharal, *Phys. Rev. B: Condens. Matter Mater. Phys.*, 2000, **62**, 10000–10003.
35 D. Cappelletti, E. Ronca, L. Belpassi, F. Tarantelli and F. Pirani, *Acc. Chem. Res.*, 2012, **45**, 1571–1580.
36 L. Jaberansari, M. G. Hahm, S. Somu, Y. Echegoyen, A. Busnaina and Y. J. Jung, *J. Am. Chem. Soc.*, 2009, **131**, 804–808.
37 X. Xiong, L. Jaberansari, M. G. Hahm, A. Busnaina and Y. J. Jung, *Small*, 2007, **3**, 2006–2010.
38 K. Balasubramanian and M. Burghard, *J. Mater. Chem.*, 2008, **18**, 3071.
39 Z. Ming and B. A. Diner, *J. Am. Chem. Soc.*, 2004, **126**, 15490.
40 B. Delley, *J. Chem. Phys.*, 1990, **92**, 508; *J. Chem. Phys.*, 2000, **113**, 7756.
41 J. P. Perdew, K. Burke and M. Ernzerhof, *Phys. Rev. Lett.*, 1996, **77**, 3865.
42 J. Baker, *J. Comput. Chem.*, 1986, **7**(4), 385.
43 C. J. Cerjan and W. H. Miller, *J. Chem. Phys.*, 1981, **75**, 2800.
44 N. Govind, M. Petersen, G. Fitzgerald, D. King-Smith and J. Andzelm, *Comput. Mater. Sci.*, 2003, **28**, 250.
45 V. Jeena and R. S. Robinson, *Chem. Commun.*, 2012, **48**, 299–301.
46 T. Saito, Y. Nishiyama, J. Putaux, M. Vignon and A. Isogai, *Biomacromolecules*, 2006, **7**, 1687–1691.
47 Y. Jing, J. Jiang, B. Yan, S. Lu, J. Jiao, H. Xue, G. Yang and G. Zheng, *Adv. Synth. Catal.*, 2011, **353**(7), 1146–1152.
48 Y. Wang, X. Song, S. Shao, H. Zhong and F. Lin, *RSC Adv.*, 2012, **2**, 7693–7698.
49 K. Balasubramanian and M. Burghard, *J. Mater. Chem.*, 2008, **18**, 3071–3083.
50 Z. Ming and B. A. Diner, *J. Am. Chem. Soc.*, 2004, **126**, 15490–15494.
51 V. Derycke, R. Martel, J. Appenzeller and P. Avouris, *Nano Lett.*, 2001, **1**, 453–456.
52 P. G. Collins, K. Bradley, M. Ishigami and A. Zettl, *Science*, 2000, **287**, 1801–1804.
53 T. A. Halgren and W. N. Lipscomb, *Chem. Phys. Lett.*, 1977, **49**, 225–232.